ACS OMEGA

http://pubs.acs.org/journal/acsodf

Article

Zn(II)-tetracarboxy-phthalocyanine-Sensitized TiO_2 Thin Films as Antimicrobial Agents under Visible Irradiation: a Combined DFT and Experimental Study

William Vallejo,* Karen Navarro, Carlos Díaz-Uribe, Eduardo Schott, Ximena Zarate,* and Eduard Romero

Cite This: *ACS Omega* 2021, 6, 13637−13646

Read Online

ACCESS | Metrics & More | Article Recommendations | Supporting Information

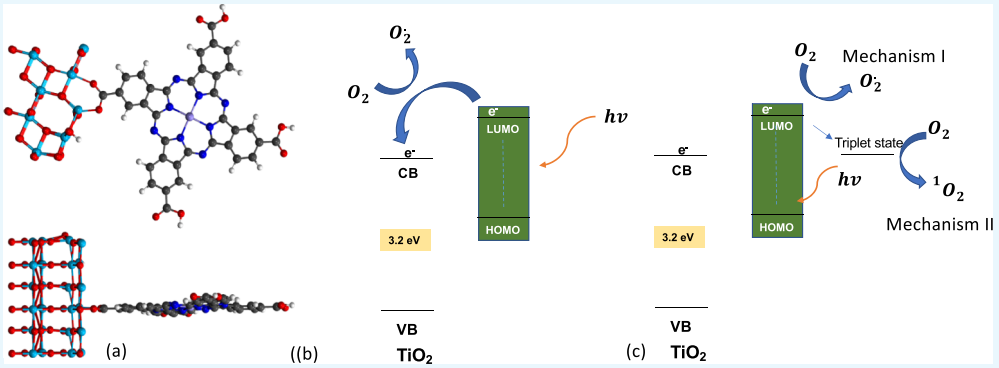

ABSTRACT: In this article, we studied the antimicrobial activity of TiO_2 sensitized by the Zn(II)-tetracarboxy-phthalocyanine (TcPcZn) complex using TiO_2-Degussa P25 as a semiconductor source. The TiO_2 thin films were deposited by the doctor blade method and were sensitized by the chemisorption process. The obtained compounds were characterized using Fourier transform infrared spectroscopy, UV−vis spectrophotometry, Raman spectroscopy, diffuse reflectance spectroscopy, and scanning electron microscopy. Furthermore, we studied the stability of the adsorbed sensitizer on the semiconductor surface by using the density functional theory (DFT). Additionally, we determined the antimicrobial activity of TcPcZn−TiO_2 against methicillin-resistant *Staphylococcus aureus* (MRSA). The Raman and optical results confirmed the sensitizing process. The TcPcZn−TiO_2 thin films showed radiation absorption in the visible range of the electromagnetic spectrum (600−750 nm), and the dye anchored on the TiO_2 surface had a band gap of 1.58 eV. The DFT study showed that TcPcZn supported on any phase of Degussa P25 is stable, making them suitable to act as catalysts in the proposed reactions. Finally, the TcPcZn−TiO_2 thin films reached 76.5% of inhibition activity against MRSA.

1. INTRODUCTION

Methicillin-resistant *Staphylococcus aureus* (MRSA) bacteria are a public health problem.[1,2] Reports estimate that in the first decade of this century, in United States alone, nearly 20,000 people died and more than 500,000 were hospitalized due to infections caused by these bacteria.[3,4] The infections caused by such bacteria through skin-to-skin contact are typical in hospital settings, primarily among healthcare workers and patients; therefore, the risk of infection and spreading among doctors, nurses, or other healthcare professionals and patients is continuous.[5] *S. aureus* bacteria are resistant to some conventional antibiotics (*e.g.*, penicillin derivatives such as methicillin, cephalosporins, and vancomycin). During the last few decades, research on new developments in the field of antibiotics has been conducted to find alternatives for the control of resistant pathogenic microorganisms.[6−8] Various nanomaterials have antimicrobial properties that are not found in their micro-/macrocounterparts (silver nanoparticles are an example); however, technical challenges (*e.g.*, agglomeration and loss of antibacterial activity over time) limit their commercial application.[9,10] Nowadays, advanced oxidation processes (AOPs) involving metal oxides have emerged as an alternative degradation technology both to eliminate recalcitrant compounds from wastewater and to inactivate bacteria and viruses in different types of environments.[11] Different semiconductors, derivatives, and mixtures thereof have shown

Received: February 4, 2021
Accepted: May 10, 2021
Published: May 20, 2021

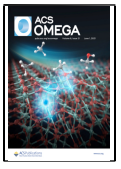

Table 1. Reports on Antimicrobial Activities of Different Semiconductors

semiconductor/reference	microorganism	antimicrobial activity (best result)[a]
SnO_2, SnS_2, and SnO_2/SnS_2[12]	*Escherichia coli* (ATCC 25922) and *Staphylococcus aureus* (ATCC 6538)	reduction of 73% of cfu of *E. coli* and reduction of 70% of cfu of *S. aureus*
ZnO[13]	*Escherichia coli* and *Staphylococcus aureus*	25% of bacterial reduction (*E. coli*) and 50% of bacterial reduction (*S. aureus*)
TiO^2 thin films[14]	*Escherichia coli*	100% of lethality under UV light irradiation after 20 min
TiO_2/ZnO[15]	*Staphylococcus aureus*, *Pseudomonas fluorescens*, *Listeria monocytogenes*, and *Escherichia coli O157:H7*	FIC (mg/mL)[b], 0.33 against *S. aureus* and *P. fluorescens*, 0.40 against *L. monocytogenes*, and 0.25 against *E. coli*.
Cu_2O/r-GO[c]16	*Escherichia coli* and *Staphylococcus aureus*	70% of bacterial reduction of *E. coli* and 65% of bacterial reduction of *S. aureus*
TiO_2/*Garcinia zeylanica extract*[17]	MRSA was investigated under light irradiation	reduction of 99.1% of cfu under sunlight exposure
TiO_2/5,10,15,20-tetrakis(2,6-difluorosulfonylophenyl)porphyrin[18]	*Staphylococcus aureus* was investigated under light irradiation	(>6 log killing) under visible irradiation
TiO_2/Procion Red[19]	*Staphylococcus aureus* (ATCC25923) was investigated under light irradiation	99% under visible irradiation

[a]Authors reported many tests, but we cited the best result from each reference. [b]FCI: fractional inhibitory concentration. [c]r-GO: stable reduced graphene oxide.

their potential as antimicrobial agents, and the list includes SnO_2, SnS_2, Cu_2O, ZnO, TiO_2/graphene, and its derivatives. Table 1 compiles information on this topic for different types of semiconductors.

Among metal-oxide semiconductors, TiO_2 has been recognized as the most promising photocatalyst owing to its unique electronic configuration, photostability, cost, and nontoxicity.[20] Different authors have stressed that TiO_2 is useful in the degradation of various bacteria.[21,22] Matsunaga first published a study on the photocatalytic inactivation of microorganisms using TiO_2 nanoparticles.[23] Azizi-Lalabadi *et al.* reported the antimicrobial activity of TiO_2 nanoparticles supported in zeolite.[15] Ripolles-Avila *et al.* reported bactericidal activity against Gram-positive and Gram-negative bacteria by TiO_2 nanoparticles under UV irradiation.[24] Kubacka *et al.* presented a complete study of TiO_2 films as antimicrobial agents against a pathogenic bacterium.[25] Nevertheless, TiO_2 is catalytically active only under UV irradiation, a fact that restricts its application under direct solar irradiation, as only 4% of solar spectrum radiation is located in the UV region. Nowadays, solar photocatalytic applications are part of green strategies (clean and cheap photochemical technologies) to improve wastewater and antimicrobial treatments; furthermore, the solar photocatalytic wastewater treatment shows great potential for practical applications.[26] In the last decade, different methodologies have been attempted to improve TiO_2 photoactivity in the visible region (*e.g.*, doping,[27−30] semiconductor coupling,[31−33] transition-metal coupling,[34−36] and sensitization with both synthetic[37,38] and natural dyes[39−42]). Among such strategies, the use of synthetic dyes as sensitizers is an efficient process for TiO_2 modification. Sensitization improves the absorption of visible light, improving the photocatalytic activity under visible irradiation. The physicochemical process relies on electron transfer at the sensitizer/semiconductor interface—a similar process occurs in dye-sensitized solar cells.[43,44] Currently, N_4 macrocycles (*e.g.*, phthalocyanines and porphyrins) have demonstrated their advantages given their low cost and their special physical−chemical properties to convert visible light into chemical energy.[45,46] Phthalocyanines exhibit some attractive properties, namely: (i) high absorption coefficients in the visible region, (ii) high photostability, and (iii) strongly bonded to the TiO_2 surface through carboxylate groups (when this group is present).[47,48] Therefore, phthalocyanines are promising candidates for antimicrobial application (*e.g.*, heterogeneous photocatalysis and photodynamic therapy).[49−52] Phthalocyanines have proved their potential as photosensitizers of TiO_2. Altin *et al.* reported the photocatalytic removal of methyl orange and under visible irradiation on zinc phthalocyanine-sensitized TiO_2 nanocomposites.[53] Cobalt phthalocyanine−TiO_2 nanocomposites were used in the photodegradation of organic textile dyes.[54] In this context, the surface functionalization of TiO_2 has potential to be an effective photocatalytic agent on a wide range of microorganisms and chemical contaminants under visible light radiation. Currently, heterogeneous photocatalysis aims at the development of a solar photocatalytic treatment. In the present study, we carried out theoretical and experimental studies of Zn(II)-tetracarboxyphthalocyanine (TcPcZn)-sensitized TiO_2 thin films regarding their antimicrobial activity against MRSA under visible irradiation.

2. RESULTS AND DISCUSSION

2.1. Structural Study. The TiO_2 semiconductor has three crystalline structures: rutile, anatase, and brookite. Although the rutile-TiO_2 phase is the most thermodynamically stable one, the anatase-TiO_2 has higher photocatalytic activity. Both the anatase and rutile crystalline structures can be built as chains of TiO_6 octahedral, the difference between both chemical structures is the distortion of the octahedra and the binding pattern of their chains along the crystal lattice; because of that, they present different physicochemical properties (*e.g.*, recombination rates, band gaps, photocatalytic activity, and so forth).[55,56]

Figure 1 shows experimental X-ray diffraction patterns for the thin films studied. The XRD-TiO_2 pattern showed typical signals corresponding to anatase (JCPDS #071-1166) and rutile (JCPDS #021-1276) crystalline phases. The presence of both crystalline phases is due to the TiO_2 source (Degussa P25).[57,58] The TiO_2 powder (Degussa, P-25), a standard material in the field of photocatalytic reactions, contains anatase and rutile phases in a ratio of about 3:1; this composition is typical and has been reported by other authors with regard to its photocatalytic applications.[59] After the sensitizing process, the diffraction pattern did not change significantly. Furthermore, none of the films showed any evidence of the presence of other phases, which is a result aligned with other reports.[60] The thin-film-crystal-domain size was determined using the Debye−Scherrer equation and the full width at half maximum (fwhm) for the signal (101). The

https://doi.org/10.1021/acsomega.1c00658
ACS Omega 2021, 6, 13637−13646

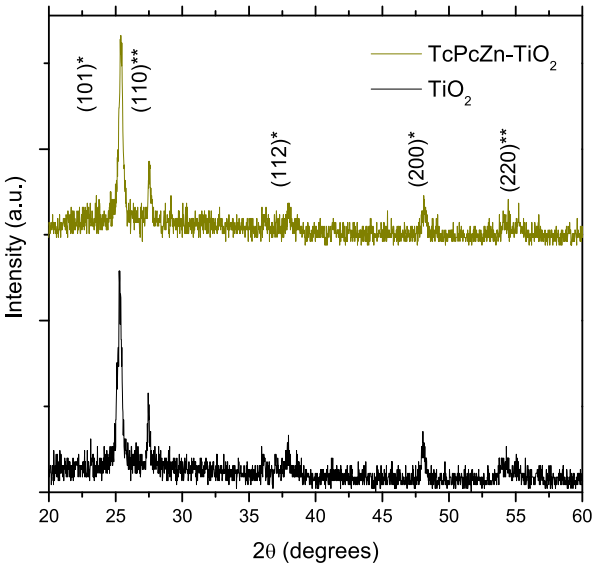

Figure 1. X-ray diffraction patterns for the catalysts synthesized in this study, where (*) indicates signals for the anatase phase and (**) for the rutile crystalline phase.

average crystal size was 21.5 nm for TiO_2 and 20.8 nm for TcPcZn−TiO_2 thin films.

2.2. Morphological Study. Figure 2 displays the scanning electron microscopy (SEM) images obtained for TiO_2 and

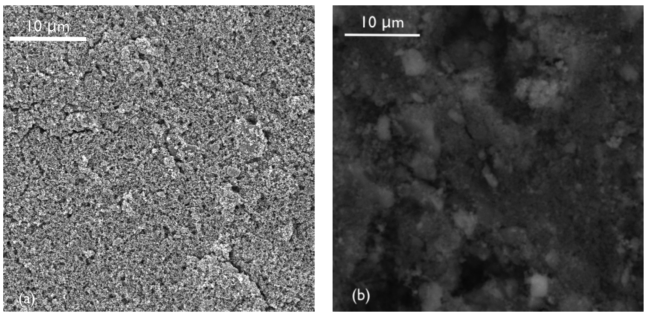

Figure 2. SEM images of (a) TiO_2 films and (b) TcPcZn−TiO_2 films.

TcPcZn−TiO_2 thin films. Figure 2a shows formed micro-aggregates with a narrow size margin of 50-100 nm for the TiO_2 films, which is a common result for the TiO_2 Degussa P25 used in thin-film fabrication.[61] Figure 2b shows that the morphological properties of the semiconductor surface changed after the sensitizing process. Thus, the micro-aggregates of the TcPcZn−TiO_2 film shows a larger grain size than the TiO_2 films; some reports point out that the aggregation of TcPcZn on the TiO_2 surface after the adsorption process is possible.[62] Moreover, in the first stages of the sensitizing process, the dye tends to occupy the spaces with greater surface energy on TiO_2 (free spaces on the surface). Finally, this result is in agreement with other reports.[63,64]

2.3. Raman Study. The Raman spectra of a typical dye (*e.g.*, ruthenium complexes for DSSC applications) have been studied for characterization of their chemical structures and their adsorption on the TiO_2 surface.[65−68] Figure 3a shows the Raman spectrum for TiO_2 thin films; the signals located at 144 and 639 cm^{-1} are assigned to the E_{1g} vibrational mode; the signal located at 518 cm^{-1} is assigned to the A_g vibrational

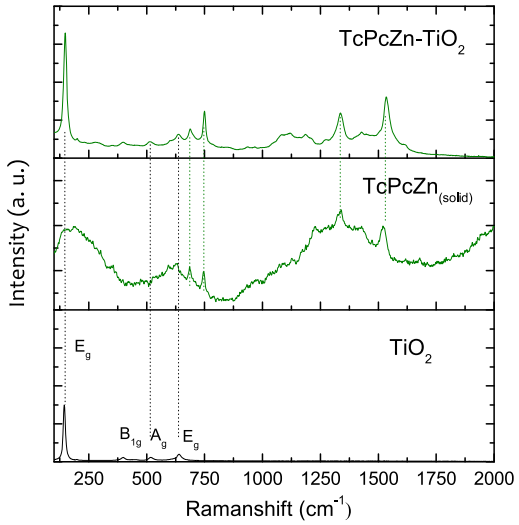

Figure 3. Raman spectra for the catalysts fabricated in this study: free TiO_2, free TcPcZn, and TcPcZn−TiO_2.

mode; and the signal located at 398 cm^{-1} is assigned to the B_{1g} vibrational mode—all these signals correspond to TiO_2.[69] Figure 3b shows the free TcPcZn (solid state) Raman spectrum. The results show signals located at 1545, 1337, 751, and 641 cm^{-1}, with these vibration modes corresponding to bonding C_β−C_β vibrations of the pyrrole, isoindole, and symmetric and asymmetric distortions of the macrocycle, respectively. Finally, Figure 3c shows the Raman spectrum of the TcPcZn−TiO_2 thin films; all signals observed for TcPcZn are also observed here; besides, after TcPcZn adsorption on the TiO_2 surface, Figure 3 shows how the signal assigned to the E_g vibration mode increases in its intensity, and this could be associated with surface-enhanced Raman scattering (SERS). SERS is characterized by the increase in the intensity of the signals in the Raman spectrum by several orders of magnitude due to the effect of adsorbed species on the semiconductor surface.[70] The Raman results allowed observing that TcPcZn was adsorbed on the TiO_2 thin films; this will also be supported with the obtained optical results.

2.4. Optical Study. Figure 4a shows the diffuse reflectance spectrum of the thin films. As can be observed, TiO_2 did not show optical activity in the visible region, and this behavior is in concordance with the high-energy band gap value of TiO_2.[71] In contrast, the TcPcZn−TiO_2 thin films showed optical activity in the visible region (from 600 to 750 nm). Furthermore, Figure 4a shows two new signals (639 and 711 nm), which can be associated with (n → π^*) transitions and are commonly reported for metal phthalocyanine compounds.[72] The band gap energy values for all photocatalytic systems (TcPcZn−TiO_2) were determined for all samples using the Kubelka−Munk remission function,[73] and the analogue to Tauc plots $(F(R_\infty)h\nu)^{1/2}$ against photon energy can be made according to[74]

$$(F(R_\infty)h\nu)^{1/2} = A(h\nu - E_g) \quad (1)$$

Figure 4b shows the plots of $(F(R_\infty)h\nu)^{1/2}$ *versus* $(h\nu)$, which allows determining the band gap of films.[75] Figure 4b shows that TiO_2 thin films have a band gap value of 3.06 eV, a value that is in concordance with previous reports (3.10 eV for Degussa P25).[76]

https://doi.org/10.1021/acsomega.1c00658
ACS Omega 2021, 6, 13637−13646

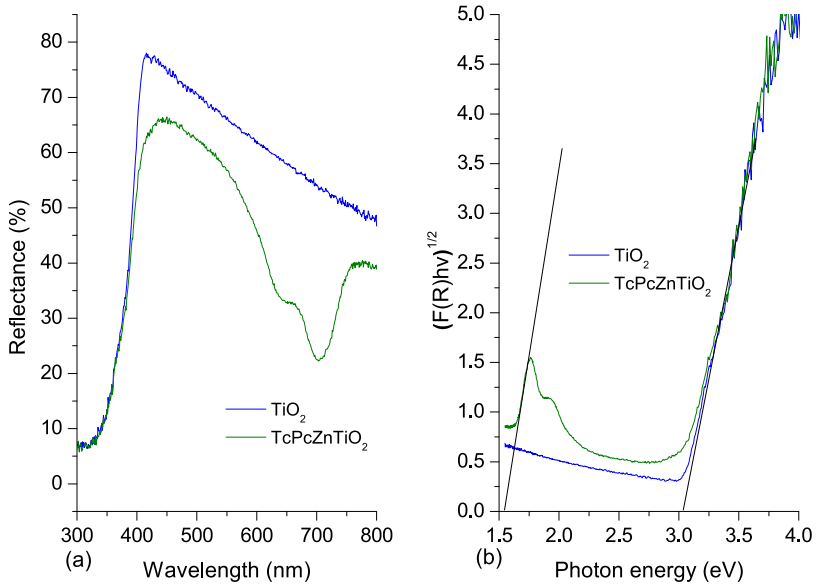

Figure 4. (a) UV−vis diffuse reflectance spectra and (b) Kubelka−Munk plots and band gap energy estimation for both the TiO_2 and TcPcZn−TiO_2 thin films.

The dye anchored on the TiO_2 surface (TcPcZn−TiO_2 films) has a band gap value of 1.58 eV. As observed, after the sensitizing process, the optical properties of TcPcZn−TiO_2 films in the visible region improved significantly, which also suggests that after the sensitizing process this type of film could work as a catalyst under visible irradiation.[77]

2.5. Antimicrobial Activity against MRSA. Figure 5 shows the antimicrobial activity of both catalysts. Bare-TiO_2 did not affect the inhibition of MRSA when visible light was used as an irradiation source, this result is in concordance with the previously reported TiO_2. In general, no toxic effect was found without irradiation. The photodynamically induced death of bacteria was dependent on the type of material and irradiation light, this is according to the photodynamic process requirement.[18] The TcPcZn−TiO_2 thin films reached 76.5% of inhibition activity against MRSA. The positive control (ciprofloxacin) reached 80.2% of inhibition activity.

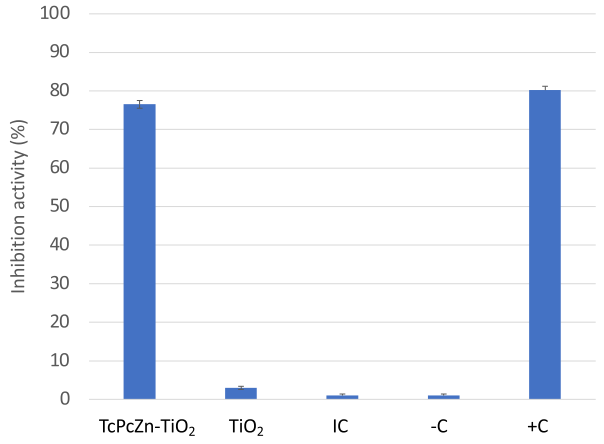

Figure 5. Results of inhibition activity against MRSA for TiO_2 and TcPcZn−TiO_2 thin films. IC (irradiation control), −C (negative control), and +C (positive control).

These results are significant compared with other reports in the literature. Table 1 lists reports of antimicrobial activities of TiO_2 with different surface modifications. The comparison of these results against the TiO_2 modified with a natural product (*Garcinia zeylanica extract*), which has inherent antimicrobial activity, indicates that phthalocyanine is a potential sensitizer for this kind of application. In a recent study, Sułek *et al.* reported antimicrobial activity against Gram-positive *S. aureus* and Gram-negative *Escherichia coli* bacteria of the system TiO_2/5,10,15,20-tetrakis(2,6-difluorosulfonylphenyl)porphyrin and its zinc derivative. They found that the photoinactivation of both systems can eradicate (>6 log killing) *S. aureus*, whereas no bactericidal effect was obtained against Gram-negative *E. coli*.[18] Other types of dyes have also been tested as sensitizers. Krishna *et al.* reported the use of two azo dyes (Mordant Orange and Procion Red) as sensitizers of TiO_2 to inactivate *S. aureus* (ATCC25923) under visible irradiation.[19] Such antimicrobial activity can be explained by the following: (i) after visible absorption, phthalocyanine undergoes excitation, promoting an electron from the HOMO to the LUMO. This electron is injected into the conduction band of TiO_2. Afterward, this electron can react to generate reactive oxygen species (ROS)[78−80]

$$\text{TcPcZn} - \text{TiO}_2 + h\nu_{(E>E_g)} \rightarrow \text{TcPcZn}^* - \text{TiO}_2 \quad (2)$$

$$\text{TcPcZn}^* - \text{TiO}_2 \rightarrow \text{TcPcZn}^+ - \text{TiO}_2(e^-_{cb}) \quad (3)$$

$$(e^-_{cb}) + O_{2(ad)} \rightarrow O_2^{\bullet -} \quad (4)$$

$$O_2^{\bullet -} + H_2\vec{O}OH^{\bullet} + OH^- + \frac{1}{2}O_2 \quad (5)$$

After the electron transfer, ROS (c.a. O_2^-) are generated and the conventional photocatalytic process starts, with the consequent degradation of *MRSA*; (ii) after visible absorption, the excited electron located on the LUMO of the phthalocyanine could decay, generating hydroxyl or superoxide radicals (type I mechanism) or singlet oxygen (type II mechanism). In either case, the generated ROS are highly cytotoxic for *MRSA*[81−85]

https://doi.org/10.1021/acsomega.1c00658
ACS Omega 2021, 6, 13637−13646

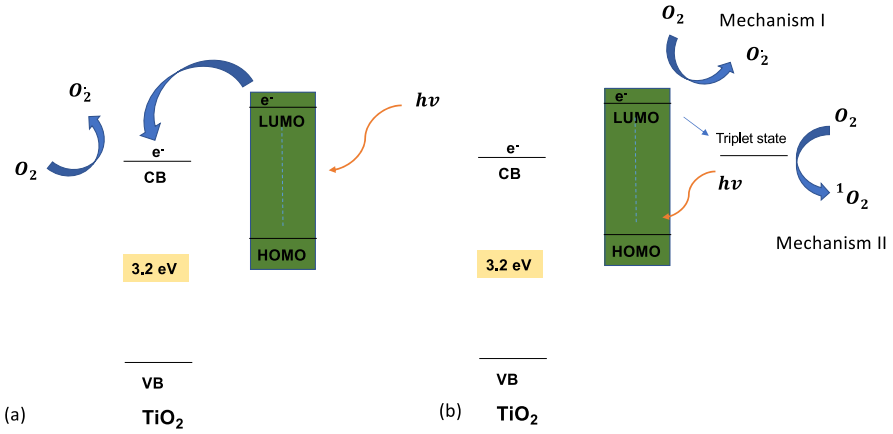

Figure 6. HOMO−LUMO transition level of phthalocyanine and the energetic level of the semiconductor. (a) Conventional ROS generation by electron transfer from the LUMO dye state to TiO_2 (see eqs 2−5). (b) ROS generation of the dye through mechanism I (electron transfer) and through mechanism II (energy-transfer reaction) (see eqs 6 and 7).

$$\text{TcPcZn}^* - \text{TiO}_2 + \text{O}_2 \rightarrow \text{TcPcZn}^+ - \text{TiO}_2 + \text{O}_2^{\bullet -} \quad (6)$$

$$\text{TcPcZn}^* - \text{TiO}_2 + \text{O}_2 \rightarrow \text{TcPcZn}^+ - \text{TiO}_2 + {}^1\text{O}_2 \quad (7)$$

Figure 6 shows the HOMO−LUMO transition level of phthalocyanine and the energetic level of the semiconductor, indicating the possible ROS generation mechanism.

2.6. DFT Results. The TcPcZn macrocycle adsorbed on the semiconductor surface was modeled in the periodic-DFT framework using plane waves. The anatase and rutile structures were both studied and chosen as the crystalline TiO_2-Degussa P25 (employed in the present experiments), constituting both phases in the films. Therefore, slab models of the anatase and rutile phases were constructed with $(TiO_2)_{24}$ units. The molecular structure of the sensitizer was first optimized in the gas phase and isolated. Subsequently, the molecule was monodeprotonated (the hydrogen atom of one −COOH group was abstracted) and the $-COO^-$ group was placed close to the slab, facing the Ti atoms at a distance of 1.5 Å to allow the energy and structure optimizations of an adsorbed system through chemical interactions. The obtained results show the bidentate binuclear anchoring form of TcPcZn with anatase TiO_2 nanoparticles, where the bond lengths between the carboxylic oxygens with Ti atoms are 2.411 and 2.015 Å (see Figure 7a). In the case of rutile, a monodentate mononuclear interaction between the sensitizer and the semiconductor was observed, with a bond length of 2.12 Å, as shown in Figure 7b. For both systems, the hydrogen that migrated to the semiconductor forms a bond with an oxygen of the exposed layer of the TiO_2 model. On the other hand, the adsorption energies (E_{ads}) were calculated using eq 1 (see the Computational Methods section). The E_{ads} for the adsorbed systems with the anatase structure is −62.18 kcal/mol, whereas using the rutile phase, the E_{ads} is −50.01 kcal/mol, thus evidencing that considerable interaction and stable adsorption promote electronic coupling between the TcPcZn and the TiO_2-nanostructured films and resulting in efficient sensitization. Furthermore, there was a difference regarding the optimized structures, where, in the case of the anatase phase, a full planarity of the macrocycle and the carboxylic acid that bond to the structure was observed. On the other hand, in the case of the rutile phase, an almost 90° rotation between the macrocycle and the carboxylic acid bond to the structure was observed. In this way, both observed facts (bidentate *vs* monodentate bonding and the torsion angle between the macrocycle and the carboxylic acid) support the lower adsorption energy observed for rutile in comparison with anatase.

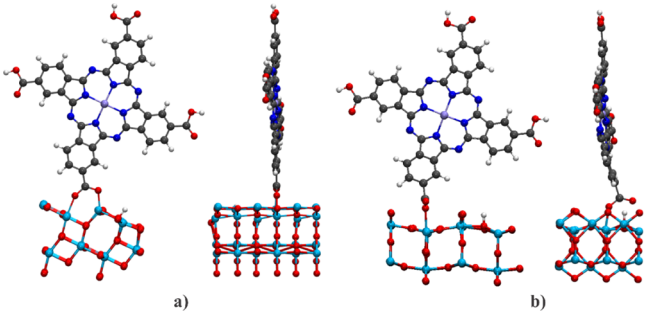

Figure 7. Adsorbed TcPcZn/TiO_2 systems on (a) anatase and (b) rutile phases. Color representation of the atoms: Ti atom (light blue), O atom (red), C atom (gray), H atom (white), N atom (dark blue), and Zn atom (purple).

3. CONCLUSIONS

We synthesized and characterized TcPcZn-−TiO_2 thin films. The Raman results corroborated the sensitizing process. The TcPcZn-−TiO_2 thin films showed radiation absorption at the visible range of the electromagnetic spectrum. The DFT results showed that TcPcZn supported on the phases present in Degussa P25, that is, anatase and rutile, is stable and catalytically active, where covalent interactions with the semiconductor were observed. Also, the results showed differences regarding the adsorption energies and structures in the TcPcZn/TiO_2 models. The TcPcZn-−TiO_2 thin films exhibited greater antimicrobial activity against MRSA, reaching 76.5% (±0.6) of inhibition after visible light irradiation. This behavior can be attributed to (i) ROS generation on the surface of the semiconductor and (ii) ROS generation by the sensitizer. Finally, our results indicated that TcPcZn is a suitable sensitizer for modified TiO_2 catalysts to develop an antimicrobial action under visible irradiation.

https://doi.org/10.1021/acsomega.1c00658
ACS Omega 2021, 6, 13637−13646

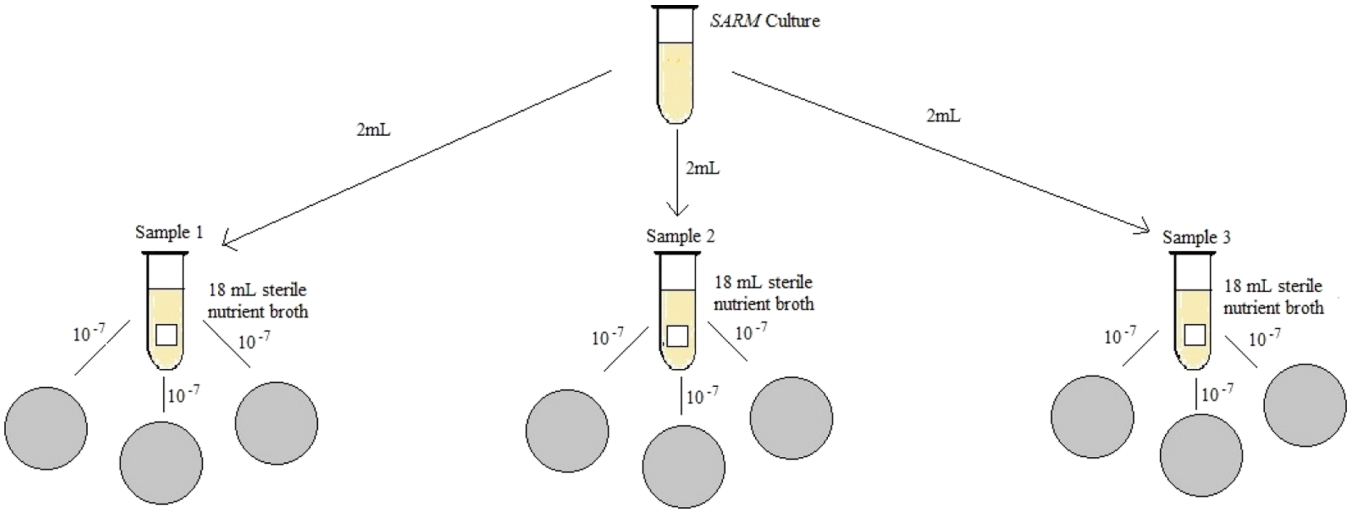

Figure 8. The cfu counting method for antimicrobial tests of thin films against MRSA. After that, tubes were irradiated under visible light for 30 min. Then, the tubes were incubated for 12 h. Adapted with permission from *Rev. Acad. Colomb. Cienc. Ex. Fis. Nat.*,[91] Copyright 2016, Rev. Acad. Colomb. Cienc. Ex. Fis. Nat.

4. EXPERIMENTAL SECTION

4.1. Synthesis and Characterization. All reagents were supplied by Merck, TiO_2 (Degussa-Nanoshel). TiO_2 thin films were deposited on soda-lime glass substrates using the doctor blade technique, and the suspension was placed on a 2 cm height by 2 cm width glass, according to previous reports.[86,87] The tetracarboxy phthalocyanines were synthesized using the method reported by Achar.[88] In summary, zinc sulfate (5.8×10^{-2} mol), trimellitic anhydride (1.8×10^{-1} mol), ammonium chloride (8.2×10^{-2} mol), and ammonium tetramolybdate (4.0×10^{-3} mol) were mixed in the solid state and, after that, the mixture was added to 10.0 mL of nitrobenzene. The mixture was heated to reflux for 4 h at 185 °C. Finally, the phthalocyanines were purified and recrystallized in an acid medium (HCl, 1.0 M). A dark-green solid was obtained. This powder was purified by means of column chromatography, using silica gel (2.5 × 24 cm) as a stationary phase and petroleum ether−ethyl acetate (15:3) as a mobile phase (rf.: 0.60); yield (35%). UV−vis (H_2SO_4) 230, 320, 630, 715 nm; FT-IR (cm^{-1}): O−H (3292−3509), C═O (1703), C═C (1525), C═N (1282); MS (ESI-IT). The infrared spectrum was measured using an ECO-ART Alpha Bruker Fourier transform infrared spectrometer. The UV−vis assay was recorded on a Shimadzu UV-2401PC UV−vis spectrophotometer. In this assay, we dissolved 2.0×10^{-4} g of dye in H_2SO_4. For phthalocyanine sensitization of the TiO_2 thin films, the previously prepared coatings were immersed in a solution of dye (1.1×10^{-1} M; pH = 5.0) and the chemical adsorption process was carried out for 24 h under constant agitation; after that, the sensitized films were washed with ethanolic solution and dried at room temperature.[42] The amount of dye adsorbed on the TiO_2 surface was determined by the sensitizer desorption for using H_2SO_4 of 98% w/w (a medium in which the dye was entirely soluble). The concentration of phthalocyanines was calculated using spectrophotometry (calibration curve at 715 nm). We determined dye adsorption (20.2×10^{-6} mol dye/g TiO_2) in more detail in the Supporting Information section. The physical−chemical properties of the films were studied by X-ray diffraction, diffuse reflectance spectrophotometry, and Raman spectroscopy. X-ray diffraction patterns were obtained with a Shimadzu 6000 diffractometer using Cu Kα radiation (λ = 0.15406 nm) as an X-ray source with a diffraction angle in the 2θ range (20−60°). Diffuse reflectance spectra were obtained with a Lambda 4 PerkinElmer spectrophotometer equipped with an integration sphere. The compositional properties of the materials were studied by Raman spectroscopy in a DXR device equipped with a 780 nm laser. The morphological properties were studied by SEM, under an excitation energy of 5 and 1 kV.[89]

4.2. Antimicrobial Activity against MRSA. We estimated viable bacteria in terms of colony-forming units (cfu)[90] based on our previous report.[91] In summary, (i) we used a nutrient broth (30.0 mL) to inoculate resistant *Staphylococcus aureus* strains (ATCC 43300). After that, the samples were stirred for 12 h at 37 °C. (ii) Then, we prepared a sample dilution until reaching 10^{-7} (see Figure 8). Subsequently, (iii) the catalyst films were plunged into the crops; and visible irradiation (450 μW cm^{-2}) was performed for 30 min. After crop irradiation, the samples were stirred for 12 h. (iv) Afterward, we determined antimicrobial activity by electronic counting of cfu in Petri dishes. Figure 8 illustrates the procedure. Furthermore, several control tests were carried out to verify the inhibitory effect caused by the photodynamic activation of TcPcZn: (a) one test consisted of a sample of TiO_2 thin films, with the strain and the nutrient broth exposed to visible light; (b) another test consisted of a sample of TcPcZn-−TiO_2 thin films, with the strain and the nutrient broth exposed to visible light; (c) the irradiation control test consisted of a sample of the TcPcZn-−TiO_2 thin film, with the strain and the nutrient broth not exposed to visible light (IC); (d) the negative control consisted of the strains and the nutrient broth (−C); and (e) the positive control (+C) consisted of the strain, the nutrient broth, and ciprofloxacin (40 mg/L). The irradiation tests were carried out in a batch reactor using an LED tape as a source of visible light radiation (cold white light, 17 W), and the incident photon flow per unit volume I_o was 5.8×10^{-7} einstein L^{-1} s^{-1}.

4.3. Computational Methods. To evaluate the stability of the adsorbed sensitizer on the semiconductor, the following procedure was carried out. A TiO_2 unit cell was modeled following the experimental parameters of a face-centered cubic

https://doi.org/10.1021/acsomega.1c00658
ACS Omega 2021, 6, 13637−13646

(fcc) crystal structure for anatase and a simple tetragonal crystal structure for rutile. Computed lattice parameters were in good agreement with those experimental values for anatase (a = 5.365 Å)[92] and rutile (a = 4.593, c = 2.959).[93] The 3 × 2 and 2 × 2 slab models were built for anatase (101) and rutile (110), respectively, from their optimized crystals. Here, two layers were used to get a slab with $(TiO_2)_{24}$ units, as shown in Figure 9. As a first step, geometry optimizations of the

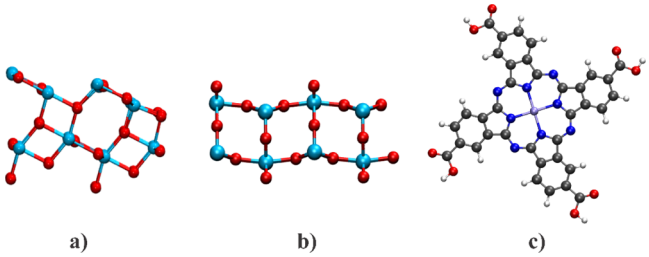

Figure 9. Semiconductor slab models: (a) anatase and (b) rutile. (c) Molecular structure of free TcPcZn. Color representation of the atoms: Ti atom (light blue), O atom (red), C atom (gray), H atom (white), N atom (dark blue), and Zn atom (purple).

semiconductors, of the TcPcZn macrocycle adsorbed onto TiO_2 (anatase and rutile) and of the free TcPcZn were performed to obtain minima structures by periodic DFT calculations, which were modeled using the Perdew–Burke–Ernzerhof (PBE) functional and GBRV 1.5 pseudopotentials.[94] An energy cutoff of 45 Ryd was employed. Particularly, a 3 × 3 × 3 k-point mesh was used to optimize the TiO_2 bulk, and the gamma point was employed to optimize the adsorbed complexes (TcPcZn/TiO_2 slab models). All extended calculations were performed with Quantum Espresso v6.4.,[95] and the images were created with VMD v1.9.3.[96] A model consisting of a single molecule per supercell was considered. Therefore, an 8 Å vacuum in the Z-axis was included, avoiding some possible interactions between the adsorbate replicas.

The starting complex geometry model consisted of TcPcZn being positioned directly onto the TiO_2 slab. The carboxylic group (−COOH) of TcPcZn was deprotonated and the proton was adsorbed in a grain boundary oxygen of the slab. Then, the $-COO^-$ group was positioned to promote an interaction between the TcPcZn oxygens and a Ti atom of the slab, considering a starting adsorbate–surface distance of ∼1.5 Å.

Afterward, due to the supercell dimensions and their high computational cost, single point calculations were performed using the same functional employed for the periodic DFT computations (PBE), the Gaussian 6-31G(d,p) basis set for nonmetal atoms (C, H, O, and N), and the pseudopotential LANL2DZ for the metals (Zn and Ti). All discrete calculations were performed using Gaussian 09.[97] For a deeper understanding of the interaction between the molecule and the semiconductor, taking into account both the semiconductor structures, the adsorption energy (E_{ads}) was calculated according to eq 8

$$E_{ads(complex)} = E_{(slab+TcPcZn)} - E_{(slab)} - E_{(TcPcZn)} \quad (8)$$

In order to get the energy values for TcPcZn (Figure 9c), the molecular structure was also optimized under extended and discrete calculations, which were carried out under the aforementioned specifications.

■ ASSOCIATED CONTENT

Supporting Information

The Supporting Information is available free of charge at https://pubs.acs.org/doi/10.1021/acsomega.1c00658.

UV–vis spectra of TcPcZn dissolved in H_2SO_4 and calibration curve (PDF)

■ AUTHOR INFORMATION

Corresponding Authors

William Vallejo − *Grupo de Investigación en Fotoquímica y Fotobiología, Programa de Química, Facultad de Ciencias Básicas, Universidad del Atlántico, Puerto Colombia 081007, Colombia*; orcid.org/0000-0002-6661-545X; Email: williamvallejo@mail.uniatlantico.edu.co

Ximena Zarate − *Instituto de Ciencias Químicas Aplicadas, Facultad de Ingeniería, Universidad Autónoma de Chile, Santiago 7500912, Chile*; Email: ximena.zarate@uautonoma.cl

Authors

Karen Navarro − *Grupo de Investigación en Fotoquímica y Fotobiología, Programa de Química, Facultad de Ciencias Básicas, Universidad del Atlántico, Puerto Colombia 081007, Colombia*

Carlos Díaz-Uribe − *Grupo de Investigación en Fotoquímica y Fotobiología, Programa de Química, Facultad de Ciencias Básicas, Universidad del Atlántico, Puerto Colombia 081007, Colombia*

Eduardo Schott − *Departamento de Química Inorgánica, Facultad de Química y de Farmacia, Centro de Energía UC, Centro de Investigación en Nanotecnología y Materiales Avanzados CIEN-UC, Pontificia Universidad Católica de Chile, 4860 Santiago, Chile; Millenium Nuclei on Catalytic Processes Towards Sustainable Chemistry (CSC), Concepcion 4030000, Chile*; orcid.org/0000-0002-2546-304X

Eduard Romero − *Departamento de Química, Universidad Nacional de Colombia, Bogotá 111321, Colombia*

Complete contact information is available at: https://pubs.acs.org/10.1021/acsomega.1c00658

Notes

The authors declare no competing financial interest.

■ ACKNOWLEDGMENTS

W.V. and C.D-U. thank Universidad del Atlántico. FONDECYT 1201880, FONDECYT 1180565 and Millennium Science Initiative of the Ministry of Economy, Development and Tourism-Chile, grant Nuclei on Catalytic Processes toward Sustainable Chemistry (CSC). ANID/FONDAP/15110019.

■ REFERENCES

(1) Dordel, J.; Kim, C.; Chung, M.; Pardos de la Gándara, M.; Holden, M. T. J.; Parkhill, J.; de Lencastre, H.; Bentley, S. D.; Tomasz, A. Novel Determinants of Antibiotic Resistance: Identification of Mutated Loci in Highly Methicillin-Resistant Subpopulations of Methicillin-Resistant Staphylococcus Aureus. *MBio* **2014**, *5*, No. e01000.

(2) de Oliveira, S. C. P. S.; Monteiro, J. S. C.; Pires-Santos, G. M.; Sampaio, F. J. P.; Soares, A. P.; Soares, L. G. P.; Pinheiro, A. L. B. LED Antimicrobial Photodynamic Therapy with Phenothiazinium Dye against Staphylococcus Aureus : An in Vitro Study. *J. Photochem. Photobiol., B* **2017**, *175*, 46–50.

(3) Kuehnert, M. J.; Hill, H. A.; Kupronis, B. A.; Tokars, J. I.; Solomon, S. L.; Jernigan, D. B. Methicillin-resistant-Staphylococcus aureusHospitalizations, United States. *Emerging Infect. Dis.* **2005**, *11*, 868−872.
(4) Klein, E.; Smith, D. L.; Laxminarayan, R. Hospitalizations and Deaths Caused by Methicillin-ResistantStaphylococcus aureus, United States, 1999-2005. *Emerging Infect. Dis.* **2007**, *13*, 1840−1846.
(5) Ki, V.; Rotstein, C. Bacterial Skin and Soft Tissue Infections in Adults: A Review of Their Epidemiology, Pathogenesis, Diagnosis, Treatment and Site of Care. *Can. J. Infect. Dis. Med. Microbiol.* **2008**, *19*, 173.
(6) Chambers, H. F.; DeLeo, F. R. Waves of Resistance: Staphylococcus Aureus in the Antibiotic Era. *Nat. Rev. Microbiol.* **2009**, *7*, 629−641.
(7) Rayner, C.; Munckhof, W. J. Antibiotics Currently Used in the Treatment of Infections Caused by Staphylococcus Aureus. *Intern. Med. J.* **2005**, *35*, S3−S16.
(8) Kaur, D.; Chate, S. Study of Antibiotic Resistance Pattern in Methicillin Resistant Staphylococcus Aureus with Special Reference to Newer Antibiotic. *J. Global Infect. Dis.* **2015**, *7*, 78−84.
(9) Wong, K. K. Y.; Liu, X. Silver Nanoparticles - The Real "Silver Bullet" in Clinical Medicine? *Medchemcomm* **2010**, *1*, 125−131.
(10) Díez-Pascual, A. M. Antibacterial Action of Nanoparticle Loaded Nanocomposites Based on Graphene and Its Derivatives: A Mini-Review. *Int. J. Mol. Sci.* **2020**, *21*, 3563.
(11) Dizaj, S. M.; Lotfipour, F.; Barzegar-Jalali, M.; Zarrintan, M. H.; Adibkia, K. Antimicrobial Activity of the Metals and Metal Oxide Nanoparticles. *Mater. Sci. Eng., C* **2014**, *44*, 278−284.
(12) Fakhri, A.; Behrouz, S.; Pourmand, M. Synthesis, Photocatalytic and Antimicrobial Properties of SnO2, SnS2 and SnO2/SnS2 Nanostructure. *J. Photochem. Photobiol., B* **2015**, *149*, 45−50.
(13) El-Nahhal, I. M.; Salem, J.; Anbar, R.; Kodeh, F. S.; Elmanama, A. Preparation and Antimicrobial Activity of ZnO-NPs Coated Cotton/Starch and Their Functionalized ZnO-Ag/Cotton and Zn(II) Curcumin/Cotton Materials. *Sci. Rep.* **2020**, *10*, 5410.
(14) Joost, U.; Juganson, K.; Visnapuu, M.; Mortimer, M.; Kahru, A.; Nõmmiste, E.; Joost, U.; Kisand, V.; Ivask, A. Photocatalytic Antibacterial Activity of Nano-TiO2 (Anatase)-Based Thin Films: Effects on Escherichia Coli Cells and Fatty Acids. *J. Photochem. Photobiol., B* **2015**, *142*, 178−185.
(15) Azizi-Lalabadi, M.; Ehsani, A.; Divband, B.; Alizadeh-Sani, M. Antimicrobial Activity of Titanium Dioxide and Zinc Oxide Nanoparticles Supported in 4A Zeolite and Evaluation the Morphological Characteristic. *Sci. Rep.* **2019**, *9*, 17439.
(16) Yang, Z.; Hao, X.; Chen, S.; Ma, Z.; Wang, W.; Wang, C.; Yue, L.; Sun, H.; Shao, Q.; Murugadoss, V.; Guo, Z. Long-Term Antibacterial Stable Reduced Graphene Oxide Nanocomposites Loaded with Cuprous Oxide Nanoparticles. *J. Colloid Interface Sci.* **2019**, *533*, 13−23.
(17) Senarathna, U. L. N. H.; Fernando, S. S. N.; Gunasekara, T. D. C. P.; Weerasekera, M. M.; Hewageegana, H. G. S. P.; Arachchi, N. D. H.; Siriwardena, H. D.; Jayaweera, P. M. Enhanced Antibacterial Activity of TiO2 Nanoparticle Surface Modified with Garcinia Zeylanica Extract. *Chem. Cent. J.* **2017**, *11*, 7.
(18) Sułek, A.; Pucelik, B.; Kuncewicz, J.; Dubin, G.; Dąbrowski, J. M. Sensitization of TiO2 by Halogenated Porphyrin Derivatives for Visible Light Biomedical and Environmental Photocatalysis. *Catal. Today* **2019**, *335*, 538−549.
(19) Krishna, V.; Bai, W.; Han, Z.; Yano, A.; Thakur, A.; Georgieva, A.; Tolley, K.; Navarro, J.; Koopman, B.; Moudgil, B. Contaminant-Activated Visible Light Photocatalysis. *Sci. Rep.* **2018**, *8*, 1894.
(20) Yemmireddy, V. K.; Hung, Y.-C. Using Photocatalyst Metal Oxides as Antimicrobial Surface Coatings to Ensure Food Safety-Opportunities and Challenges. *Compr. Rev. Food Sci. Food Saf.* **2017**, *16*, 617−631.
(21) Pham, T.-D.; Lee, B.-K. Disinfection of Staphylococcus Aureus in Indoor Aerosols Using Cu-TiO2 Deposited on Glass Fiber under Visible Light Irradiation. *J. Photochem. Photobiol., A* **2015**, *307−308*, 16−22.
(22) Meng, D.; Liu, X.; Xie, Y.; Du, Y.; Yang, Y.; Xiao, C. Antibacterial Activity of Visible Light-Activated TiO2 Thin Films with Low Level of Fe Doping. *Adv. Mater. Sci. Eng.* **2019**, *2019*, 5819805.
(23) Matsunaga, T. Sterilization with Particule Photosemiconductor. *J. Antibact. Antifungal Agents* **1985**, *13*, 211−220.
(24) Ripolles-Avila, C.; Martinez-Garcia, M.; Hascoët, A.-S.; Rodríguez-Jerez, J. J. Bactericidal Efficacy of UV Activated TiO2 Nanoparticles against Gram-Positive and Gram-Negative Bacteria on Suspension. *CyTA–J. Food* **2019**, *17*, 408−418.
(25) Kubacka, A.; Diez, M. S.; Rojo, D.; Bargiela, R.; Ciordia, S.; Zapico, I.; Albar, J. P.; Barbas, C.; Martins Dos Santos, V. A. P.; Fernández-García, M.; Ferrer, M. Understanding the antimicrobial mechanism of TiO2-based nanocomposite films in a pathogenic bacterium. *Sci. Rep.* **2014**, *4*, 4134.
(26) Colmenares, J. C. Selective Redox Photocatalysis: Is There Any Chance for Solar Bio-Refineries? *Curr. Opin. Green Sustain. Chem.* **2019**, *15*, 38−46.
(27) Rasoulnezhad, H.; Hosseinzadeh, G.; Yekrang, J. Preparation and Characterization of Nanostructured S and Fe Co-Doped TiO 2 Thin Film by Ultrasonic-Assisted Spray Pyrolysis Method. *J. Nanostruct.* **2018**, *8*, 251−258.
(28) Diaz-Uribe, C.; Vallejo, W.; Ramos, W. Methylene Blue Photocatalytic Mineralization under Visible Irradiation on TiO2 Thin Films Doped with Chromium. *Appl. Surf. Sci.* **2014**, *319*, 121−127.
(29) Cravanzola, S.; Cesano, F.; Gaziano, F.; Scarano, D.; Cravanzola, S.; Cesano, F.; Gaziano, F.; Scarano, D. Sulfur-Doped TiO2: Structure and Surface Properties. *Catalysts* **2017**, *7*, 214.
(30) Kuriakose, S.; Satpati, B.; Mohapatra, S. Enhanced Photocatalytic Activity of Co Doped ZnO Nanodisks and Nanorods Prepared by a Facile Wet Chemical Method. *Phys. Chem. Chem. Phys.* **2014**, *16*, 12741.
(31) Vallejo, W.; Díaz-Uribe, C.; Rios, K. Methylene Blue Photocatalytic Degradation under Visible Irradiation on In2S3 Synthesized by Chemical Bath Deposition. *Adv. Phys. Chem.* **2017**, *2017*, 1−5.
(32) Loh, K.; Gaylarde, C. C.; Shirakawa, M. A. Photocatalytic Activity of ZnO and TiO2 "Nanoparticles" for Use in Cement Mixes. *Constr. Build. Mater.* **2018**, *167*, 853−859.
(33) Rawal, S. B.; Bera, S.; Lee, D.; Jang, D.-J.; Lee, W. I. Design of Visible-Light Photocatalysts by Coupling of Narrow Bandgap Semiconductors and TiO2: Effect of Their Relative Energy Band Positions on the Photocatalytic Efficiency. *Catal. Sci. Technol.* **2013**, *3*, 1822.
(34) Díaz-Uribe, C.; Viloria, J.; Cervantes, L.; Vallejo, W.; Navarro, K.; Romero, E.; Quiñones, C. Photocatalytic Activity of Ag-TiO2 Composites Deposited by Photoreduction under UV Irradiation. *Int. J. Photoenergy* **2018**, *2018*, 1−8.
(35) Türkyılmaz, Ş. Ş.; Güy, N.; Özacar, M. Photocatalytic Efficiencies of Ni, Mn, Fe and Ag Doped ZnO Nanostructures Synthesized by Hydrothermal Method: The Synergistic/Antagonistic Effect between ZnO and Metals. *J. Photochem. Photobiol., A* **2017**, *341*, 39−50.
(36) Ayati, A.; Ahmadpour, A.; Bamoharram, F. F.; Tanhaei, B.; Mänttäri, M.; Sillanpää, M. A Review on Catalytic Applications of Au/TiO2 Nanoparticles in the Removal of Water Pollutant. *Chemosphere* **2014**, *107*, 163−174.
(37) Ghazal, B.; Azizi, K.; Ewies, E. F.; Youssef, A. S. A.; Mwalukuku, V. M.; Demadrille, R.; Torres, T.; Makhseed, S. Push-Pull Zinc Phthalocyanine Bearing Hexa-Tertiary Substituted Carbazolyl Donor Groups for Dye-Sensitized Solar Cells. *Molecules* **2020**, *25*, 1692.
(38) Pirbazari, A. E. Sensitization of Tio2 Nanoparticles With Cobalt Phthalocyanine: An Active Photocatalyst for Degradation of 4-Chlorophenol under Visible Light. *Procedia Mater. Sci.* **2015**, *11*, 622−627.
(39) Díaz-Uribe, C.; Vallejo, W.; Campos, K.; Solano, W.; Andrade, J.; Muñoz-Acevedo, A.; Schott, E.; Zarate, X. Improvement of the photocatalytic activity of TiO 2 using Colombian Caribbean species (Syzygium cumini) as natural sensitizers: Experimental and theoretical studies. *Dyes Pigm.* **2018**, *150*, 370−376.

https://doi.org/10.1021/acsomega.1c00658
ACS Omega 2021, 6, 13637−13646

(40) Litter, M. I.; San Román, E.; Grela, t. l. M. A.; Meichtry, J. M.; Rodríguez, H. B. Sensitization of TiO2 by Dyes: A Way to Extend the Range of Photocatalytic Activity of TiO2 to the Visible Region. *Visible Light-Active Photocatalysis*; Wiley-VCH Verlag GmbH & Co. KGaA: Weinheim, Germany, 2018; pp 253−282.
(41) Vallejo, W.; Rueda, A.; Díaz-Uribe, C.; Grande, C.; Quintana, P. Photocatalytic activity of graphene oxide-TiO 2 thin films sensitized by natural dyes extracted from Bactris guineensis. *R. Soc. Open Sci.* **2019**, *6*, 181824.
(42) Diaz-Uribe, C.; Vallejo, W.; Camargo, G.; Muñoz-Acevedo, A.; Quiñones, C.; Schott, E.; Zarate, X. Potential use of an anthocyanin-rich extract from berries of Vaccinium meridionale Swartz as sensitizer for TiO2 thin films - An experimental and theoretical study. *J. Photochem. Photobiol., A* **2019**, *384*. DOI: 10.1016/j.jphotochem.2019.112050.
(43) Richhariya, G.; Kumar, A.; Tekasakul, P.; Gupta, B. Natural Dyes for Dye Sensitized Solar Cell: A Review. *Renew. Sustain. Energy Rev.* **2017**, *69*, 705−718.
(44) Pelaez, M.; Nolan, N. T.; Pillai, S. C.; Seery, M. K.; Falaras, P.; Kontos, A. G.; Dunlop, P. S. M.; Hamilton, J. W. J.; Byrne, J. A.; O'Shea, K.; Entezari, M. H.; Dionysiou, D. D. A Review on the Visible Light Active Titanium Dioxide Photocatalysts for Environmental Applications. *Appl. Catal., B* **2012**, *125*, 331−349.
(45) Huang, Z.; Zheng, B.; Zhu, S.; Yao, Y.; Ye, Y.; Lu, W.; Chen, W. Photocatalytic activity of phthalocyanine-sensitized TiO2-SiO2 microparticles irradiated by visible light. *Mater. Sci. Semicond. Process.* **2014**, *25*, 148−152.
(46) Luna-Flores, A.; Valenzuela, M. A.; Luna-López, J. A.; Hernández de la Luz, A. D.; Muñoz-Arenas, L. C.; Méndez-Hernández, M.; Sosa-Sánchez, J. L. Synergetic Enhancement of the Photocatalytic Activity of TiO2 with Visible Light by Sensitization Using a Novel Push-Pull Zinc Phthalocyanine. *Int. J. Photoenergy* **2017**, *2017*, 1604753.
(47) Chen, Z.; Zhou, S.; Chen, J.; Li, L.; Hu, P.; Chen, S.; Huang, M. An Effective Zinc Phthalocyanine Derivative for Photodynamic Antimicrobial Chemotherapy. *J. Lumin.* **2014**, *152*, 103−107.
(48) Denes, G. Phthalocyanines: Properties and Applications, Volume 4 Edited by C. C. Leznoff and A. B. P. Lever (York University, Canada). VCH: New York, 1996. vi + 524 pp. $150.00. ISBN 1-56081-916-2. *J. Am. Chem. Soc.* **1998**, *120*, 241−242.
(49) Liu, Q.; Pang, M.; Tan, S.; Wang, J.; Chen, Q.; Wang, K.; Wu, W.; Hong, Z. Potent Peptide-Conjugated Silicon Phthalocyanines for Tumor Photodynamic Therapy. *J. Canc.* **2018**, *9*, 310−320.
(50) Li, X.; Lee, S.; Yoon, J. Supramolecular Photosensitizers Rejuvenate Photodynamic Therapy. *Chem. Soc. Rev.* **2018**, *47*, 1174−1188.
(51) Vallejo, W.; Cantillo, A.; Díaz-Uribe, C. Methylene Blue Photodegradation under Visible Irradiation on Ag-Doped ZnO Thin Films. *Int. J. Photoenergy* **2020**, *2020*, 1627498.
(52) Vallejo, W.; Diaz-Uribe, C.; Cantillo, Á. Methylene Blue Photocatalytic Degradation under Visible Irradiation on TiO2 Thin Films Sensitized with Cu and Zn Tetracarboxy-Phthalocyanines. *J. Photochem. Photobiol., A* **2015**, *299*, 80−86.
(53) Altın, İ.; Sökmen, M.; Bıyıklıoğlu, Z. Quaternized Zinc(II) Phthalocyanine-Sensitized TiO2: Surfactant-Modified Sol−Gel Synthesis, Characterization and Photocatalytic Applications. *Desalin. Water Treat.* **2016**, *57*, 16196−16207.
(54) Dindaş, G. B.; Şahin, Z.; Cengiz Yatmaz, H.; Işçi, Ü. Cobalt Phthalocyanine-TiO 2 Nanocomposites for Photocatalytic Remediation of Textile Dyes under Visible Light Irradiation. *J. Porphyr. Phthalocyanines* **2019**, *23*, 561−568.
(55) Li, W.; Ni, C.; Lin, H.; Huang, C. P.; Shah, S. I. Size dependence of thermal stability of TiO2 nanoparticles. *J. Appl. Phys.* **2004**, *96*, 6663−6668.
(56) Zhang, J.; Sun, P.; Jiang, P.; Guo, Z.; Liu, W.; Lu, Q.; Cao, W. The formation mechanism of TiO2 polymorphs under hydrothermal conditions based on the structural evolution of [Ti(OH)h(H2O)6−h]4−h monomers. *J. Mater. Chem. C* **2019**, *7*, 5764−5771.
(57) Tetteh, E. K.; Rathilal, S.; Naidoo, D. B. Photocatalytic Degradation of Oily Waste and Phenol from a Local South Africa Oil Refinery Wastewater Using Response Methodology. *Sci. Rep.* **2020**, *10*, 8850.
(58) Li, S.; Zhao, Z.; Huang, Y.; Di, J.; Jia, Y.; Zheng, H. Hierarchically Structured WO3-CNT@TiO2NS Composites with Enhanced Photocatalytic Activity. *J. Mater. Chem. A* **2015**, *3*, 5467−5473.
(59) Fujishima, A.; Zhang, X.; Tryk, D. TiO2 Photocatalysis and Related Surface Phenomena. *Surf. Sci. Rep.* **2008**, *63*, 515−582.
(60) Mali, S. S.; Shinde, P. S.; Betty, C. A.; Bhosale, P. N.; Lee, W. J.; Patil, P. S. Nanocoral Architecture of TiO2 by Hydrothermal Process: Synthesis and Characterization. *Appl. Surf. Sci.* **2011**, *257*, 9737−9746.
(61) Azizah, N.; Hashim, U.; Arshad, M. K. M.; Gopinath, S. C. B.; Nadzirah, S.; Farehanim, M. A.; Fatin, M. F.; Ruslinda, A. R.; Ayub, R. M. Surface Morphology of Titanium Dioxide (TiO2) Nanoparticles on Aluminum Interdigitated Device Electrodes (IDEs). *AIP Conf. Proc.* **2016**, *1733*, 020079.
(62) He, J.; Hagfeldt, A.; Lindquist, S.-E.; Grennberg, H.; Korodi, F.; Sun, L.; Åkermark, B. Phthalocyanine-Sensitized Nanostructured TiO2Electrodes Prepared by a Novel Anchoring Method. *Langmuir* **2001**, *17*, 2743−2747.
(63) Ashokkumar, R.; Kathiravan, A.; Ramamurthy, P. Zn-Phthalocyanine-Functionalized Nanometal and Nanometal-TiO2 Hybrids: Aggregation Behavior and Excited-State Dynamics. *Phys. Chem. Chem. Phys.* **2014**, *16*, 14139−14149.
(64) Mangialardo, S.; Larciprete, M. C.; Belardini, A.; Sibilia, C.; Bertolotti, M. Determination of the Aggregation Degree of Zinc-Phthalocyanines Derivatives into Polymeric Films via the Characterization of the Linear-Optical Absorption. *Laser Phys.* **2008**, *18*, 1371−1377.
(65) Likodimos, V.; Stergiopoulos, T.; Falaras, P.; Harikisun, R.; Desilvestro, J.; Tulloch, G. Prolonged Light and Thermal Stress Effects on Industrial Dye-Sensitized Solar Cells: A Micro-Raman Investigation on the Long-Term Stability of Aged Cells. *J. Phys. Chem. C* **2009**, *113*, 9412−9422.
(66) Nazeeruddin, M. K.; Müller, E.; Humphry-Baker, R.; Vlachopoulos, N.; Grätzel, M. Redox Regulation in Ruthenium(II) Polypyridyl Complexes and Their Application in Solar Energy Conversion. *J. Chem. Soc., Dalton Trans.* **1997**, 4571−4578.
(67) Falaras, P.; Gratzel, M.; Goff, A. H. L.; Nazeeruddin, M.; Vrachnou, E. Dye Sensitization of TiO2 Surfaces Studied by Raman Spectroscopy. *J. Electrochem. Soc.* **1993**, *140*, L92.
(68) Nagai, S.; Hirano, G.; Bessho, T.; Satori, K. Raman Spectroscopic Study of Dye Adsorption on TiO2 Electrodes of Dye-Sensitized Solar Cells. *Vib. Spectrosc.* **2014**, *72*, 66−71.
(69) Justh, N.; Bakos, L. P.; Hernádi, K.; Kiss, G.; Réti, B.; Erdélyi, Z.; Parditka, B.; Szilágyi, I. M. Photocatalytic Hollow TiO2 and ZnO Nanospheres Prepared by Atomic Layer Deposition. *Sci. Rep.* **2017**, *7*, 4337.
(70) Yang, L.; Gong, M.; Jiang, X.; Yin, D.; Qin, X.; Zhao, B.; Ruan, W. Investigation on SERS of different phase structure TiO2 nanoparticles. *J. Raman Spectrosc.* **2015**, *46*, 287−292.
(71) Naldoni, A.; Riboni, F.; Guler, U.; Boltasseva, A.; Shalaev, V. M.; Kildishev, A. V. Solar-Powered Plasmon-Enhanced Heterogeneous Catalysis. *Nanophotonics* **2016**, *5*, 112.
(72) Machado, A. E. H.; França, M. D.; Velani, V.; Magnino, G. A.; Velani, H. M. M.; Freitas, F. S.; Müller, P. S., Jr; Sattler, C.; Schmücker, M. Characterization and Evaluation of the Efficiency of TiO2/Zinc Phthalocyanine Nanocomposites as Photocatalysts for Wastewater Treatment Using Solar Irradiation. *Int. J. Photoenergy* **2008**, *2008*, 482373.
(73) Simmons, E. L. Relation of the Diffuse Reflectance Remission Function to the Fundamental Optical Parameters. *Opt. Acta Int. J. Opt.* **1972**, *19*, 845−851.
(74) Viezbicke, B. D.; Patel, S.; Davis, B. E.; Birnie, D. P. Evaluation of the Tauc Method for Optical Absorption Edge Determination:

ZnO Thin Films as a Model System. *Phys. Status Solidi* **2015**, *252*, 1700−1710.
(75) Pal, M.; Pal, U.; Jiménez, J. M. G. Y.; Pérez-Rodríguez, F. Effects of Crystallization and Dopant Concentration on the Emission Behavior of TiO2:Eu Nanophosphors. *Nanoscale Res. Lett.* **2012**, *7*, 1.
(76) Guayaquil-Sosa, J. F.; Serrano-Rosales, B.; Valadés-Pelayo, P. J.; de Lasa, H. Photocatalytic Hydrogen Production Using Mesoporous TiO2 Doped with Pt. *Appl. Catal., B* **2017**, *211*, 337−348.
(77) Batista, P. S.; De Souza, D. R.; Maximiano, R. V.; Barbosa Neto, N. M.; Machado, A. E. H. Quantum Efficiency of Hydroxyl Radical Formation in a Composite Containing Nanocrystalline TiO2 e Zinc Phthalocyanine, and the Nature of the Incident Radiation. *J. Mater. Sci. Res.* **2013**, *2*, p82.
(78) Schneider, J.; Matsuoka, M.; Takeuchi, M.; Zhang, J.; Horiuchi, Y.; Anpo, M.; Bahnemann, D. W. Understanding TiO2Photocatalysis: Mechanisms and Materials. *Chem. Rev.* **2014**, *114*, 9919−9986.
(79) Duncan, W. R.; Stier, W. M.; Prezhdo, O. V. AbInitioNonadiabatic Molecular Dynamics of the Ultrafast Electron Injection across the Alizarin−TiO2Interface. *J. Am. Chem. Soc.* **2005**, *127*, 7941−7951.
(80) Herrmann, J.-M. Heterogeneous photocatalysis: state of the art and present applications In honor of Pr. R.L. Burwell Jr. (1912-2003), Former Head of Ipatieff Laboratories, Northwestern University, Evanston (Ill). *Top. Catal.* **2005**, *34*, 49−65.
(81) Mafukidze, D. M.; Mashazi, P.; Nyokong, T. Synthesis and Singlet Oxygen Production by a Phthalocyanine When Embedded in Asymmetric Polymer Membranes. *Polymer* **2016**, *105*, 203−213.
(82) Nwahara, N.; Britton, J.; Nyokong, T. Improving Singlet Oxygen Generating Abilities of Phthalocyanines: Aluminum Tetrasulfonated Phthalocyanine in the Presence of Graphene Quantum Dots and Folic Acid. *J. Coord. Chem.* **2017**, *70*, 1601−1616.
(83) Granados-Oliveros, G.; Páez-Mozo, E. A.; Martínez Ortega, F.; Piccinato, M.; Silva, F. N.; Guedes, C. L. B.; Di Mauro, E.; Costa, M. F. d.; Ota, A. T. Visible light production of superoxide anion with MCarboxyphenylporphyrins (M=H, Fe, Co, Ni, Cu, and Zn) free and anchored on TiO2: EPR characterization. *J. Mol. Catal. A Chem.* **2011**, *339*, 79−85.
(84) Zarate, X.; Schott-Verdugo, S.; Rodriguez-Serrano, A.; Schott, E. The Nature of the Donor Motif in Acceptor-Bridge-Donor Dyes as an Influence in the Electron Photo-Injection Mechanism in DSSCs. *J. Phys. Chem. A* **2016**, *120*, 1613−1624.
(85) Schweitzer, C.; Mehrdad, Z.; Noll, A.; Grabner, E.-W.; Schmidt, R. Mechanism of Photosensitized Generation of Singlet Oxygen during Oxygen Quenching of Triplet States and the General Dependence of the Rate Constants and Efficiencies of O2(1Σg+), O2(1Δg), and O2(3Σg-) Formation on Sensitizer Triplet State Energy and Oxidation Potential. *J. Phys. Chem. A* **2003**, *107*, 2192−2198.
(86) Quiñones, C.; Ayala, J.; Vallejo, W. Methylene Blue Photoelectrodegradation under UV Irradiation on Au/Pd-Modified TiO2 Films. *Appl. Surf. Sci.* **2010**, *257*, 367−371.
(87) Patiño-Camelo, K.; Diaz-Uribe, C.; Gallego-Cartagena, E.; Vallejo, W.; Martinez, V.; Quiñones, C.; Hurtado, M.; Schott, E. Cyanobacterial Biomass Pigments as Natural Sensitizer for TiO2 Thin Films. *Int. J. Photoenergy* **2019**, *2019*, 1−9.
(88) Achar, B. N.; Fohlent, G. M.; Parker, J. A.; Keshavayya, J. Preparation and Structural Investigations of Copper(II), Cobalt(II), Nickel(II) and Zinc(II) Derivatives of 2,9,16,23-Phthalocyanine Tetracarboxylic Acid. *Indian J. Chem.* **1988**, *27*, 411−416.
(89) Vallejo, W.; Cantillo, A.; Salazar, B.; Diaz-Uribe, C.; Ramos, W.; Romero, E.; Hurtado, M. Comparative Study of ZnO Thin Films Doped with Transition Metals (Cu and Co) for Methylene Blue Photodegradation under Visible Irradiation. *Catalysts* **2020**, *10*, 528.
(90) Shrivastava, S.; Bera, T.; Roy, A.; Singh, G.; Ramachandrarao, P.; Dash, D.; Shrivastava, S. Characterization of Enhanced Antibacterial Effects of Novel Silver Nanoparticles. *Nanotechnol* **2007**, *18*, 225103.
(91) Vallejo, W.; Díaz-Uribe, C.; Navarro, K.; Valle, R.; Arboleda, J. W.; Romero, E. Estudio de la actividad antimicrobiana de películas delgadas de dióxido de titanio modificado con plata. *Rev. Acad. Colomb. Cienc. Exactas Fis. Nat.* **2016**, *40*, 69.
(92) Horn, H.; Schwerdtfeger, C. F.; Meagher, E. P. Refinement of the Structure of Anatase at Several Temperatures *. *Z. Kristallogr.* **1972**, *136*, 273−281.
(93) Meagher, E. P.; Lager, G. A. Polyhedral Thermal Expansion in the TiO 2 Polymorphs; Refinement of the Crystal Structures of Rutile and Brookite at High Temperature. *Can. Mineral.* **1979**, *17*, 77−85.
(94) Garrity, K. F.; Bennett, J. W.; Rabe, K. M.; Vanderbilt, D. Pseudopotentials for High-Throughput DFT Calculations. *Comput. Mater. Sci.* **2014**, *81*, 446−452.
(95) Giannozzi, P.; Baroni, S.; Bonini, N.; Calandra, M.; Car, R.; Cavazzoni, C.; Ceresoli, D.; Chiarotti, G. L.; Cococcioni, M.; Dabo, I.; Dal Corso, A.; de Gironcoli, S.; Fabris, S.; Fratesi, G.; Gebauer, R.; Gerstmann, U.; Gougoussis, C.; Kokalj, A.; Lazzeri, M.; Martin-Samos, L.; Marzari, N.; Mauri, F.; Mazzarello, R.; Paolini, S.; Pasquarello, A.; Paulatto, L.; Sbraccia, C.; Scandolo, S.; Sclauzero, G.; Seitsonen, A. P.; Smogunov, A.; Umari, P.; Wentzcovitch, R. M. QUANTUM ESPRESSO: A Modular and Open-Source Software Project for Quantum Simulations of Materials. *J. Phys. Condens. Matter* **2009**, *21*, 395502.
(96) Humphrey, W.; Dalke, A.; Schulten, K. VMD: Visual Molecular Dynamics. *J. Mol. Graph.* **1996**, *14*, 33−38.
(97) Frisch, M. J.; Trucks, G. W.; Schlegel, H. B.; Scuseria, G. E.; Robb, M. A.; Cheeseman, J. R.; Scalmani, G.; Barone, V.; Mennucci, B.; Petersson, G. A.; Nakatsuji, H.; Caricato, M.; Li, X.; Hratchian, H. P.; Izmaylov, A. F.; Bloino, J.; Zheng, G.; Sonnenberg, J. L.; Hada, M.; Ehara, M.; Toyota, K.; Fukuda, R.; Hasegawa, J.; Ishida, M.; Nakajima, T.; Honda, Y.; Kitao, O.; Nakai, H.; Vreven, T.; Montgomery, J. A.; Peralta, J. E.; Ogliaro, F.; Bearpark, M.; Heyd, J. J.; Brothers, E.; Kudin, K. N.; Staroverov, V. N.; Kobayashi, R.; Normand, J.; Raghavachari, K.; Rendell, A.; Burant, J. C.; Iyengar, S. S.; Tomasi, J.; Cossi, M.; Rega, N.; Millam, J. M.; Klene, M.; Knox, J. E.; Cross, J. B.; Bakken, V.; Adamo, C.; Jaramillo, J.; Gomperts, R.; Stratmann, R. E.; Yazyev, O.; Austin, A. J.; Cammi, R.; Pomelli, C.; Ochterski, J. W.; Martin, R. L.; Morokuma, K.; Zakrzewski, V. G.; Voth, G. A.; Salvador, P.; Dannenberg, J. J.; Dapprich, S.; Daniels, A. D.; Farkas, Ö.; Foresman, J. B.; Ortiz, J. V.; Cioslowski, J.; Fox, D. J. *Gaussian 09*, Revision E.01; Gaussian, Inc.: Wallingford CT, 2009..

https://doi.org/10.1021/acsomega.1c00658
ACS Omega 2021, 6, 13637−13646